Journal of ELECTRONIC MATERIALS, Vol. 50, No. 4, 2021
https://doi.org/10.1007/s11664-020-08520-0

ASIAN CONSORTIUM ACCMS–INTERNATIONAL CONFERENCE ICMG 2020

Magnetoelectric Studies of Close-Packed and Hierarchically Ordered $CoFe_2O_4/Pb(Zr_{0.52}Ti_{0.48})O_3/La_{0.6}Sr_{0.4}MnO_3/LaNiO_3$ Multiferroic Thin Films

SRIDEVI MEENACHISUNDARAM,[1,4] NAOKI WAKIYA,[1,2,3] CHELLAMUTHU MUTHAMIZHCHELVAN,[4,6,7] PARTHASARATHI GANGOPADHYAY,[5] NAONORI SAKAMOTO,[2,3] and SURUTTAIYUDAIYAR PONNUSAMY[4]

1.—Graduate School of Science and Technology, Shizuoka University, Hamamatsu 432-8561, Japan. 2.—Department of Electronics and Materials Science, Shizuoka University, Hamamatsu 432-8561, Japan. 3.—Research Institute of Electronics, Shizuoka University, Hamamatsu 432-8561, Japan. 4.—Department of Physics and Nanotechnology, SRM Institute of Science and Technology, Chennai 603-203, India. 5.—Indira Gandhi Centre for Atomic Research, Kalpakkam, Tamil Nadu 603-102, India. 6.—e-mail: selvan.cm@srmuniv.ac.in. 7.—e-mail: selvancm@gmail.com

Enhanced magnetoelectric effects in two-dimensional multiferroics promise greater interests for fundamental understanding and for device applications. To ameliorate properties and multifunctionality of magnetoelectric materials, highly ordered multiferroic thin films ought to be optimally designed with a high surface area and with a minimum contact area between the substrate and the films. Fabrication of hierarchically ordered, hemispherical close-packed free-standing multiferroic thin film structures of $CoFe_2O_4$ (CFO)/$Pb(Zr_{0.52}Ti_{0.48})O_3$ (PZT)/$La_{0.6}Sr_{0.4}MnO_3$ (LSMO)/$LaNiO_3$ (LNO) on a Pt/Ti/SiO_2/Si substrate using a RF magnetron sputtering technique is reported here. The hemispherical space inside the shell structures, inherited from the spherical polymer, are shown by the cross-sectional scanning transmission electron microscopy. Importantly, the observed enhancement of remanent polarization is elucidated based on the facts, like the generation of a high level of compressive stress, a large thermal expansion coefficient of LSMO, and a minimal lattice mismatch with the PZT thin film.

Key words: Hemispherical structure, multiferroic thin film, polarization, magnetron sputtering

INTRODUCTION

Multiferroic composite thin films with potentially large magnetoelectric (ME) effects have attracted great research interest in the last few decades due to their multifunctional properties.[1,2] Over the past decade of ME coupling studies, both cases of polarization induced by magnetostriction and the magnetization induced by piezostriction have been observed in Cr_2O_3.[3] Most of the experimental pioneering work in ME coupling has focused on the bulk composite materials. To overcome the drawback of weak coupling due to the leakage current and to develop potential applications, a need for thin film heterostructures arises.[4] ME heterostructure thin film comprises a magnetostrictive or piezostrictive layer along with a ferromagnetic or ferroelectric layer. These separated ME heterostructures show a greater coupling response compared to single-phase materials.[5]

(Received April 9, 2020; accepted September 23, 2020; published online October 16, 2020)

In recent years, the upsurge in the development of ME devices has been remarkable among electronic components and integrated circuits.[6] Therefore, studying the coexistence of the ferroelectric and ferromagnetic phases in multiferroic thin films plays a vital role among the various multifunctional materials and their applications. Multiferroic materials have the unique property that, when subjected to an applied external magnetic field, there is a change in the electric polarization, and the application of an external electric field generates a net magnetization in the sample. The ME effect realizes the change in the electric polarization of the sample due to the application of a magnetic field.[6–9]

To enhance the ME coupling, a free-standing hemispherical shell structure was fabricated to relax the substrate clamping force between a lead zirconate titanate (PZT) thin film and the substrate.[10] In an earlier study, Reddy et al. reported that the ME coupling response was ameliorated in $BiFeO_3$ thin films after doping with transition metal ions.[11] The development of self-assembled ME devices is inevitable in the electronics industry due to their high performances. For these devices, ferroelectric material, as one of the components, has increased the device performances. Ferroelectrics are multifunctional materials that combine various properties (e.g., dielectric properties, piezoelectric properties, and pyroelectric properties) other than ferroelectricity. For further miniaturization and to improve device performances for the future, it is essential to make thin films of high quality.[12–17] Technologically, miniaturization of device characteristics become degraded because thermal expansion coefficients (TEC) of the Si substrate and ceramic thin films differ considerably. For example, the TEC of Si and PZT are 2.6×10^{-6}/K and 5.5×10^{-6}/K, respectively.[18] Therefore, when PZT ferroelectric thin film is prepared on a Si substrate, strong tensile stress is applied to the thin film. As a result, the electrical characteristics become deteriorated.[19–21] In order to improve the characteristics of PZT thin films, it has been proposed to deposit a thin buffer layer film with a TEC higher than the PZT.[22] The ferroelectric property has been increased or improved with enhanced compressive residual stress.[23] In order to increase the compressive residual stress, we introduced $LaNiO_3$ (LNO) as a buffer layer inbetween the PZT and $La_{0.6}Sr_{0.4}MnO_3$ (LSMO). The epitaxial growth of the PZT thin film also improved by using the LSMO bottom electrode along with the LNO as a buffer layer. Among the high TEC materials, LNO and LSMO for example, may be used. The TEC of LNO and LSMO are 10.0×10^{-6}/K[24] and 11.3×10^{-6}/K, respectively.[25] On the other hand, the lattice mismatch between LSMO (3.87 Å)[17] and PZT (4.04 Å)[26] is smaller compared to the lattice mismatch between LNO (3.84 Å)[26] and PZT (4.04 Å). The crystal symmetry of PZT thin film is rhombohedral. Here, we have focused on the fabrication of close-packed hemispherica-structured multiferroic thin film with a hollow space inbetween the film and the substrate. Since it has a high specific surface area, the in-plane constraint force is relaxed, and characteristics are found to be different from ordinary multiferroic thin films. Therefore, it is called a "free-standing thin film". On the other hand, the bottom electrode with high TEC leads to an improvement of the stress-mediated magnetoelectric coupling characteristics. In this research, a $CoFe_2O_4$ (CFO) layer in the free-standing multiferroic thin film applies the magnetic field and induces the electric polarization on the PZT layer; LSMO used as the bottom electrode with a large TEC is expected to enhance the magnetoelectric coupling along with the support from the buffer layer (LNO).

The ultimate goal of the present study is to reduce the clamping force and enhance the stress-mediated ME coupling mechanism in the free-standing CFO/PZT multiferroic thin film. Also, increasing the compressive stress with the assistance of the bottom electrode and buffer layer with a high TEC has been attempted. Remanent polarization has been determined from the measurement of *P–E* hysteresis loops. We also discuss the effect of applying the magnetic field for planar and free-standing multiferroic thin films. We have reported earlier that the constraint by the substrate is alleviated by the hemispherical space inside the shell.[27] It is expected to have larger ME effects in these schemes of research.

FABRICATION OF HIERARCHICALLY ORDERED HEMISPHERICAL MULTIFERROIC THIN FILM

Poly(methyl methacrylate) (PMMA) monolayer colloidal crystals with a close-packed structure were fabricated on cleaned Pt/Ti/SiO_2/Si substrates by the dip-coating method. The preparation of monolayer colloidal crystal solutions (MCCs) and stoichiometric targets of CFO, PZT, LSMO, and LNO were prepared through a solid-state reaction process, as previously described.[22] Figure 1 schematically shows each preparation stage involved in the fabrication of close-packed free-standing CFO/PZT/LSMO/LNO multiferroic thin films. Figure 1a shows the monolayer close-packed PMMA template prepared on the Pt/Ti/SiO_2/Si. In this approach, initially, we deposited lanthanum nickel oxide ($LaNiO_3$; LNO) at room temperature on the PMMA array by the self-assembly of a monolayer, subsequent RF sputtering deposition of LNO at 450°C, incinerating the PMMA template. After the removal of the MCCs, a free-standing LNO hemispherical array could be prepared. As shown in Fig. 1b, the cross-sectional image of the LNO thin film (deposited at room temperature) confirms the presence of spherical template inside the film. Figure 1c shows the LNO layer (deposited at 450°C) with the hemispherical shell structure confirming the

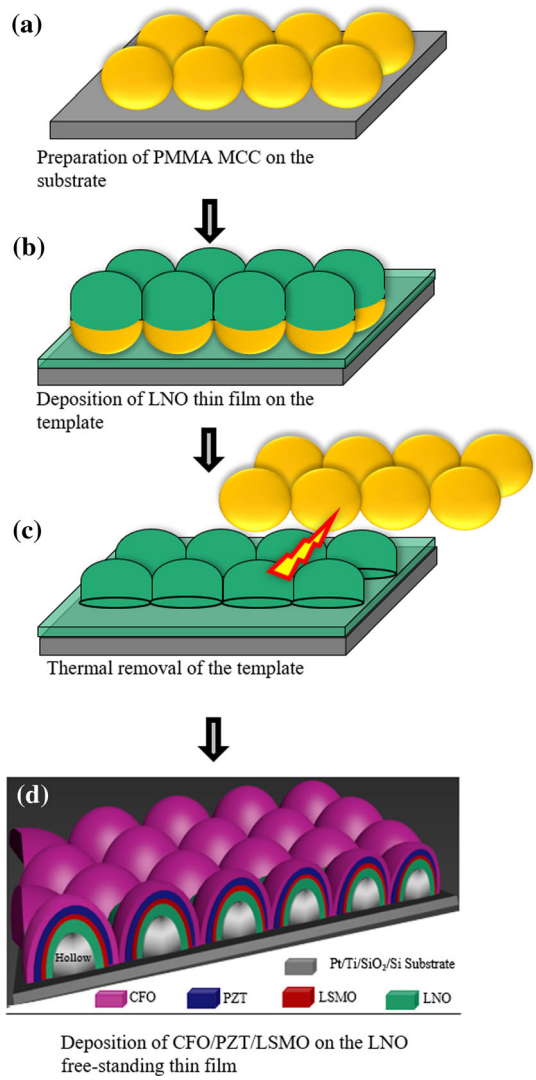

Fig. 1. Processing stages are illustrated for developing free-standing CFO/PZT/LSMO/LNO thin films on Pt/Ti/SiO_2/Si substrate. (a) Preparation of PMMA MCC on the substrate, (b) deposition of LNO thin film on the template, (c) thermal removal of the template, (d) deposition of CFO/PZT/LSMO on the LNO free-standing thin film.

spherical templates were completely removed. This LNO thin film was used as a buffer layer to enhance the crystallinity of the film. Subsequently, LSMO, PZT, and CFO were used as bottom electrode, ferroelectric, and ferromagnetic materials, respectively. Finally, the CFO/PZT/LSMO/LNO multiferroic thin films with a hollow space having a two-dimensional array of a close-packed free-standing structure was successfully fabricated, as shown in Fig. 1d. The overall surface morphology of the free-standing CFO/PZT/LSMO/LNO thin film is shown in Fig. 2a. The single shell was studied by cross-sectional scanning transmission electron microscopy (STEM; JEM-2100F; JEOL) with energy-dispersive x-ray spectroscopy (EDS) analysis (see Fig. 2). Material deposition conditions and thicknesses of each layer in the free-standing multiferroic thin film are given in Table I. Pt dots (size $\sim$ 100 μm) were deposited on the multiferroic thin film as a top electrode by RF sputtering.

CHARACTERIZATIONS

The multiferroic composite thin film crystal structure was examined by using an x-ray diffractometer (XRD; D8 Advance; Bruker). The composition and thickness of each layer were measured using x-ray fluorescence spectroscopy (Minipal; PANalytical, The Netherlands). Film morphology of the composite was recorded using scanning electron microscopy (SEM; JSM-5010LV; JEOL). The single free-standing hemispherical shell was analyzed with the cross-sectional STEM-EDS). The *M–H* loop of the composite thin film was measured using a vibrating sample magnetometer (Rigaku BHV-35). Ferroelectric polarization and magnetic field-induced polarization measurements were carried using a ferroelectric tester (FC-E; Toyo).

RESULTS AND DISCUSSION

Structural Characteristics of Free-Standing Thin Film

XRD measurements were carried out using CuKα radiation of wavelength = 1.5406 Å. XRD patterns of the free-standing hemispherical PZT/LSMO/LNO and PZT/LSMO thin films on the Pt/Ti/SiO_2/Si substrate and the corresponding XRD graph at log scale are shown in Fig. 3. Both the patterns confirm that perovskite PZT is of polycrystalline type and is preferentially oriented. The epitaxial growth of the PZT thin film was improved by using the LSMO bottom electrode along with LNO as a buffer layer.

Stress Analysis of Free-Standing Thin Film

Figure 3b shows the high-angle XRD patterns for the free-standing multiferroic thin films. The diffraction peak positions (2θ) for the PZT/LSMO and PZT/LSMO/LNO free-standing thin films are at 97.2° and 96.8°, respectively. This indicates that the crystal symmetry of the PZT thin films is pseudo-cubic (rhombohedral) for both the films. The peak position for PZT on the LSMO/LNO free-standing thin film is at the lower 2θ angle, and the peak height is higher compared to the PZT deposited on LSMO thin film. The XRD results clearly show that the crystallinity of the PZT peak and the in-plane compressive stress were enhanced with the support of LSMO along with the LNO thin film. However, we found that the diffraction peak of PZT for both cases of the free-standing thin films were shifted to a lower 2θ angle compared to the bulk PZT peak (2θ: 98.0°).[27] The peak PZT (400) shift toward the low-angle side in this ME thin film is caused by the compressive stress. The stress is generated because of the difference of the TEC between PZT and the combination of both LSMO and LNO thin films. [28,29]

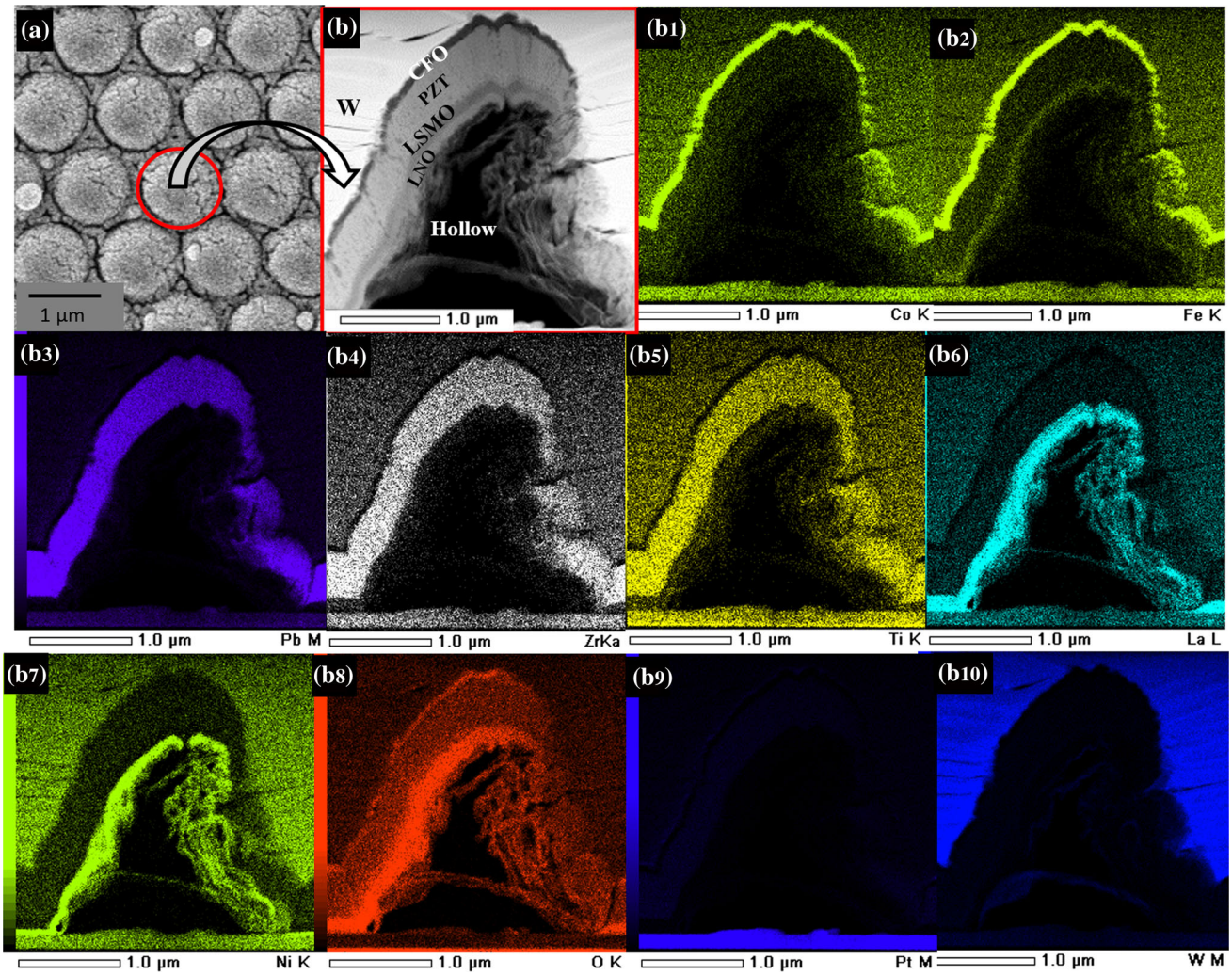

Fig. 2. (a) Surface morphology of the overall free-standing CFO/PZT/LSMO/LNO thin film. (b) Cross-sectional bright-field STEM images of a single shell and the corresponding STEM-EDS mapping of each element present in the single shell (b_1–b_{10}), respectively, are shown.

Table I. Conditions for growing free-standing CFO/PZT/LSMO/LNO multiferroic thin films using RF magnetron sputtering technique

Materials layers (nm)	Temperature (°C)	O_2 pressure (pa)	Film compositions (mol. ratio)	Materials thickness
1. LNO	RT	2	$LaNiO_3$	100
2. LNO	450	2	$LaNiO_3$	200
3. LSMO	450	2	$La_{0.6}Sr_{0.4}MnO_3$	100
3. PZT	550	3	$Pb_{1.1}(Zr_{0.52}Ti_{0.48})O_3$	360
4. CFO	700	2	$Co_{0.95}Fe_{2.05}O_4$	130

After confirming the desired crystallinity of the PZT/LSMO/LNO materials, PZT/LSMO and CFO thin films were deposited on the PZT/LSMO/LNO thin film to study the magnetoelectric properties. Figure 4 shows the XRD patterns for the free-standing CFO/PZT/LSMO/LNO multiferroic thin films. The diffraction results confirm that the prepared perovskite PZT and LNO structures were preferentially oriented. The preferred orientation of the multiferroic thin films is driven by the thermally-induced stresses. Stress is generated because of the differences in the TECs of the LSMO, LNO, and PZT materials.

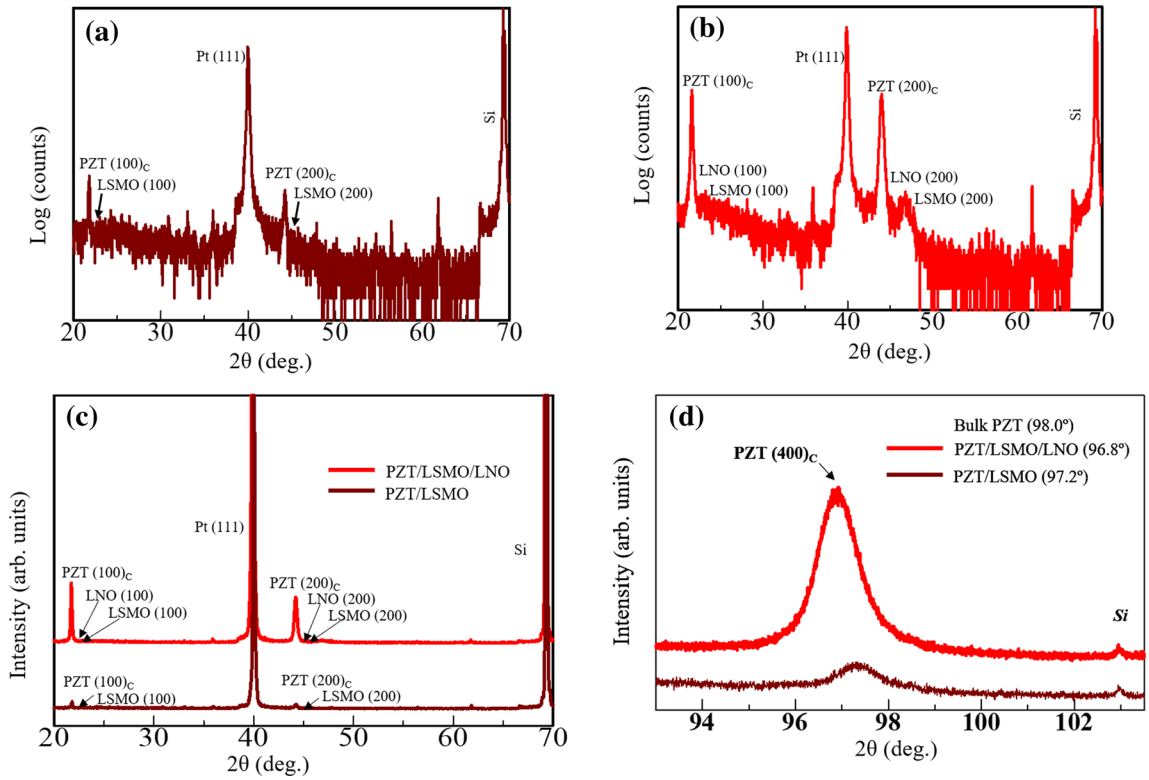

Fig. 3. X-ray diffraction patterns for (a) free-standing PZT/LSMO thin film at log scale, (b) PZT/LSMO/LNO thin film at log scale, (c) corresponding x-ray diffraction pattern, (d) high 2θ angle x-ray diffraction pattern.

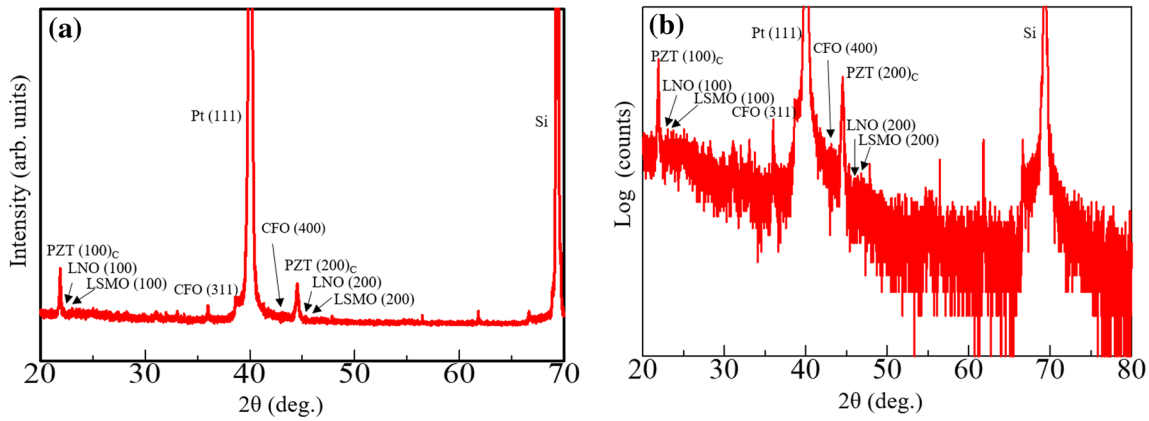

Fig. 4. (a) X-ray diffraction pattern for CFO/PZT/LSMO/LNO thin film, (b) corresponding x-ray diffraction pattern at log scale.

Magnetic Characteristics of Free-Standing Multiferroic Thin Film

Figure 5a and b shows the *M–H* curves for the CFO layer and CFO/PZT/LSMO/LNO thin films. Magnetization was measured at room temperature by applying a magnetic field up to 10 kOe. In both cases, the in-plane saturation magnetization of the free-standing thin film is smaller compared to the bulk CFO thin film. This result suggests that the CFO layer in the free-standing multiferroic thin film was more sensitive to the magnetization, and thereby enhances the magnetostrictive effect on the PZT layer.[28] Coercivity between the in-plane and out-of-plane magnetization for magnetic and multiferroic thin films were found to be the same, confirming that the input magnetic field and the thickness of the film in both cases were the same.[29] The in-plane saturation magnetization in the multiferroic thin films was reduced to 160 emu/cm^3, compared to the in-plane saturation magnetization (180 emu/cm^3) of the magnetic thin film. Therefore, it is considered that the CFO layer deposited on the PZT/LSMO/LNO layer is under tensile stress, and is expected to enhance the magnetoelectric effect. The in-plane and out-of-plane magnetic measurements were defined as the direction of the Si substrate.

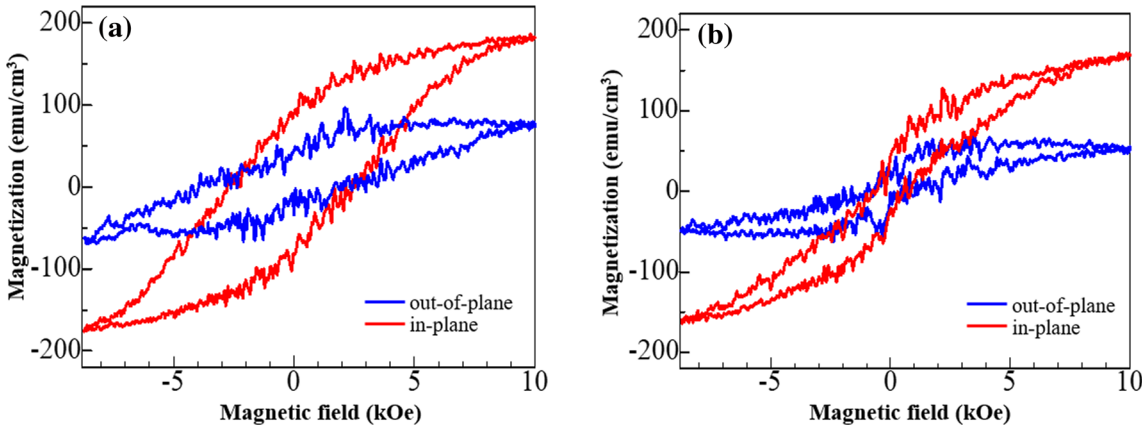

Fig. 5. (a) and (b) Show *M–H* curves for free-standing CFO and CFO/PZT/LSMO/LNO thin films, respectively.

Although each hemispherical thin film has a curved surface, the hemispherical thin films are arranged in 2D because the thin film was prepared using 2D close-packed monodisperse PMMA particles. Therefore, from the point of view of the aggregate, the hemispherical thin film can be regarded as a porous thin film. The results shown in Fig. 5b suggest a perpendicular magnetic anisotropy for the free-standing thin films. Because $CoFe_2O_4$ is of the famous perpendicular magnetic anisotropy material, the origin of the perpendicular magnetic anisotropy shown in Fig. 5b would be derived by the nature of the CFO.

Magnetoelectrical Characteristics of Free-Standing Multiferroic Thin Film

Figure 6a and b shows the schematic of the ME measurement set-up and the application of the perpendicular magnetic field on the free-standing CFO/PZT/LSMO/LNO multiferroic thin films. In this experimental set-up, a magnet is placed beside the sample; its schematic diagram is shown in Fig. 6a. A magnetic field is applied perpendicular to the sample; its schematic is shown in Fig. 6b. The magnitude of the applied external magnetic field was measured using a Gauss meter. By applying the perpendicular external magnetic field to the sample, in-plane elongation is induced on PZT by the −ve magnetostriction of the CFO. Figure 6c–f show the room-temperature ME response of the multiferroic thin films. This was measured in terms of variation of the induced voltage by the applied magnetic field. Pt was used as the top electrode, ferroelectric characteristics were measured at a frequency of 1 kHz, and a magnetic field was vertically applied to the sample. The remanent polarization changes with respect to the change of magnetic field at different voltages of 10 V, 12 V, and 15 V were measured. By increasing the applied magnetic field, as shown in Fig. 6d, the change of remanent polarization of the free-standing multiferroic film decreases for the voltages at 10 V, 12 V, and 15 V. The decreased remanent polarization of the free-standing film with respect to the external magnetic field may be explained because of the strain-induced lattice deformation in the PZT layer, and the applied magnetic field may be encouraging the magnetoelectric coupling. This causes the magnetic dipole alignment along the out-of-plane direction, which can increase the remnant polarization.[30] The increase/decrease of the coercive field by applying voltages depends on the signs of the two parameters, i.e., the magnetostrictive and piezoelectric coefficients. If both parameters are positive, the coercive field decreases. If one parameter is positive and the other is negative, the coercive field increases. Since CFO has negative magnetostriction, the coercive field increases by applying voltages.[31] In this case of multiferroic thin films, the coupling parameters develop after exposure to a magnetic field of around 1.0 kOe due to the coercivity limit of the films.[28,29] While relaxing the constraint force on the free-standing thin film structure from the substrate, it is likely to improve the ME responses of the films.

CONCLUSIONS

We report an interesting ameliorated magnetoelectric effect in CFO/PZT/LSMO/LNO multiferroic thin films with the free-standing hemispherical shell structure. An in-plane constraint force is found to be relaxed due to a smaller contact area with the substrate. Intelligent materials design and optimization of the buffer layers with large thermal expansion coefficients are found to enhance the ferroelectric behavior in the multiferroic thin films. As a result, the coexistence of the ferromagnetic and ferroelectric phases at the interface of CFO/PZT is also enhanced. Magnetic field-induced electric polarization changes in the free-standing thin film increased linearly with increasing the magnetic field, due to the strong coexistence of the perovskite PZT and spinel CFO phases in the film. In conclusion, it may be restated that multiferroic thin films

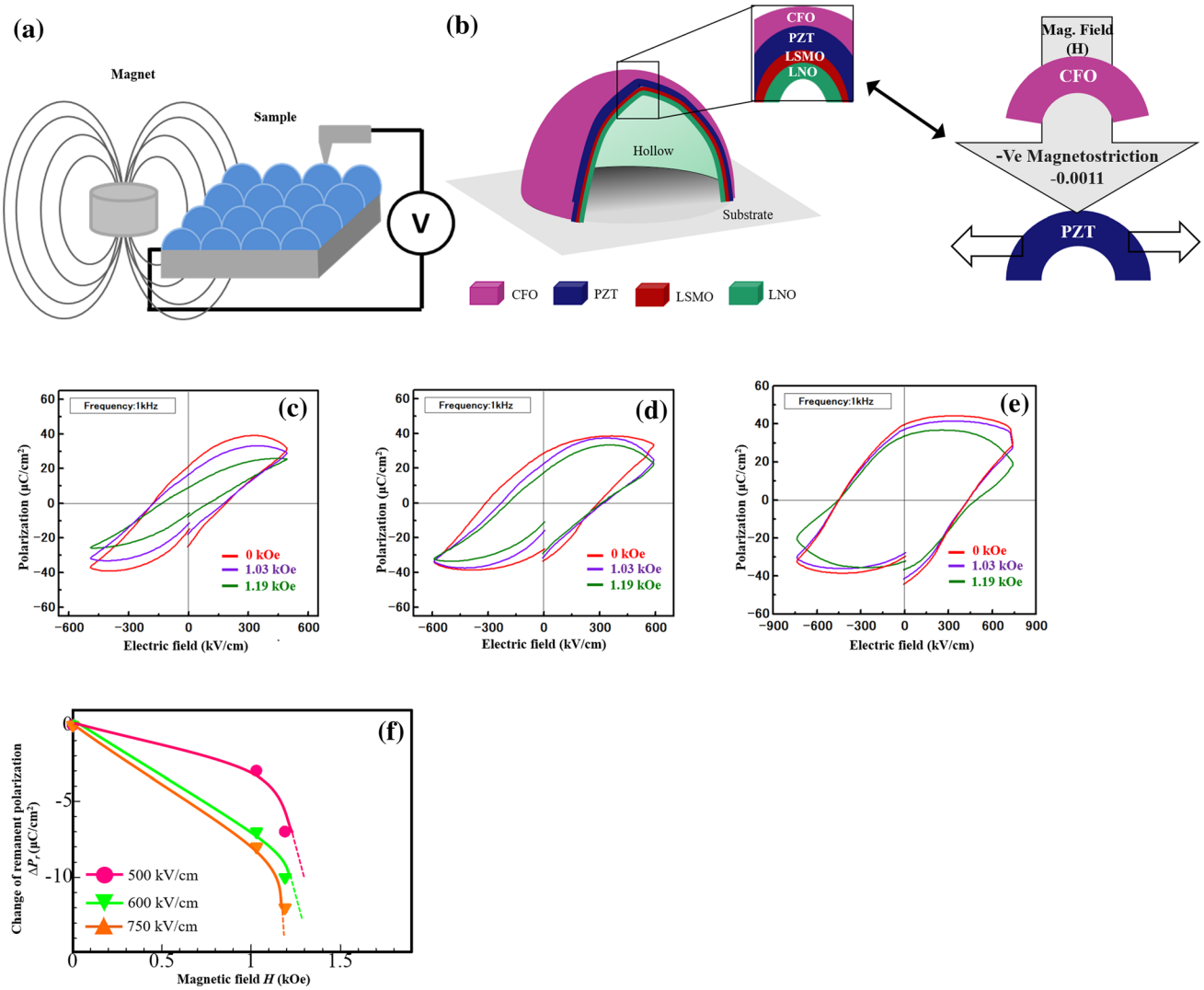

Fig. 6. Schematic illustration of the (a) ME measurement set-up, (b) application of the perpendicular magnetic field on the free-standing CFO/PZT/LSMO/LNO thin films. P-E curves are shown for applied external magnetic field perpendicular to the substrate of the corresponding thin films at (c) 500 (d) 600 and (e) 750 kV/cm. (f) Changes of remanent polarization values with the applied external magnetic field are shown.

with a novel free-standing hemispherical shell structure are expected to be one of the most promising materials with enhanced magnetoelectric effects.

CONFLICT OF INTEREST

The authors declare that they have no conflict of interest.

REFERENCES

1. J. Ma, J. Hu, Z. Li, and C.W. Nan, *Adv. Mater.* 23, 1062 (2011).
2. P. Mandal, M.J. Pitcher, J. Alaria, H. Niu, P. Borisov, P. Stamenov, J.B. Claridge, and M.J. Rosseinsky, *Nature* 525, 363 (2015).
3. V.J. Folen, G.T. Rado, and E.W. Stalder, *Phys. Rev. Lett.* 6, 607 (1961).
4. G. Lawes and G. Srinivasan, *J. Phys. D Appl. Phys.* 44, 243001 (2011).
5. Y. Cheng, B. Peng, Z. Hu, Z. Zhou, and M. Liu, *Phys. Lett. A* 382, 3018 (2018).
6. M. Mandal, S. Chatterjee, and V.R. Palkar, *J. Appl. Phys.* 110, 054313 (2011).
7. M. Vopsaroiu, J. Blackburn, and M.G. Cain, *J. Phys. D Appl. Phys.* 40, 5027 (2007).
8. A. Yourdkhani, D. Caruntu, M. Vopson, and G. Caruntu, *Cryst. Eng. Commun.* 19, 2079 (2017).
9. J.T. Evans, S.P. Chapman, S.T. Smith, B.C. Howard, and A. Gallegos, *Proceedings of IEEE-ISAF-ECAPD-PFM*, Aveiro, Portugal, July 9–13 2012.
10. S. Meenachisundaram, H. Mori, T. Kawaguchi, P. Gangopadhyay, N. Sakamoto, K. Shinozaki, C. Muthamizhchelvan, S. Ponnusamy, H. Suzuki, and N. Wakiya, *J. Alloys Compd.* 787, 1128 (2019).
11. V. Annapu Reddy, N.P. Pathak, and R. Nath, *Solid State Commun.* 171, 40 (2013).
12. E.Y. Tsymbal and H. Kohlstedt, *Science* 313, 181 (2006).
13. M. Gajek, M. Bibes, S. Fusil, K. Bouzehouane, J. Fontcuberta, A. Barthelemy, and A. Fert, *Nat. Mater.* 6, 296 (2007).
14. S. Dussan, A. Kumar, J.F. Scott, S. Priya, and R.S. Katiyar, *Appl. Phys. Lett.* 97, 252902 (2010).
15. S. Dussan, A. Kumar, R.S. Katiyar, S. Priya, and J.F. Scott, *J. Phys. Condens. Mater.* 23, 202203 (2011).
16. M. Bibes and A. Barthelemy, *Nat. Mater.* 7, 425 (2008).

17. S. Dussan, A. Kumar, J.F. Scott, and R.S. Katiyar, *Appl. Phys. Lett.* 96, 072904 (2010).
18. F. Zavaliche, H. Zheng, L.M. Ardabili, S.Y. Yang, Q. Zhan, P. Shafer, E. Reilly, R. Chopdekar, Y. Jia, P. Wright, D.G. Schlom, Y. Suzuki, and R. Ramesh, *Nano Lett.* 5, 1793 (2005).
19. F. Zavaliche, T. Zhao, H. Zheng, F. Straub, M.P. Cruz, P.L. Yang, D. Hao, and R. Ramesh, *Nano Lett.* 7, 1586 (2007).
20. H. Zheng, J. Wang, S.E. Lofland, Z. Ma, L.M. Ardabili, T. Zhao, L.S. Riba, S.R. Shinde, S.B. Ogale, F. Bai, D. Viehland, Y. Jia, D.G. Schlom, M. Wuttig, A. Roytburd, and R. Ramesh, *Science* 303, 661 (2004).
21. K. Sreenivas, M. Sayer, and P. Garrett, *Thin Sold Films* 172, 25 (1989).
22. M. Sridevi, T. Kawaguchi, R. Usami, N. Sakamoto, K. Shinozaki, C. Muthamizhchelvan, S.U. Ponnusamy, and H. Suzuki, *J. Alloys Compd.* 730, 369 (2018).
23. T. Ohno, H. Yanagida, and H. Suzuki, *J. Ceram. Soc. Japan* 122, 63 (2014).
24. Y. Tsuru, M. Shimazu, M. Shiono, and M. Moriga, *Jpn. J. Appl. Phys.* 49, 045701 (2010).
25. Y. Shirai, S. Hashimoto, K. Sato, K. Yashiro, K. Amezawa, J. Mizusaki, and T. Kawada, *Solid State Ion.* 256, 83 (2014).
26. H. Miyazakia, T. Goto, Y. Miwa, T. Ohno, H. Suzuki, T. Ota, and M. Takahashi, *J. Eur. Cer. Soc.* 24, 1005 (2004).
27. M. Nishide, H. Takeuchi, T. Tai, T. Katoda, S. Yokoyama, S. Yasui, H. Funakubo, K. Nishida, and T. Yamamoto, *Integr. Ferroelectr.* 112, 33 (2009).
28. Z. Li, Y. Gao, B. Yang, Y. Lin, R. Yu, and C.W. Nan, *J. Am. Ceram. Soc.* 94, 1060 (2011).
29. J.P. Zhou, H.C. He, Z. Shi, and C.W. Nan, *J. Appl. Phys.* 88, 013111 (2006).
30. J.X. Zhang, J.Y. Dai, C.K. Chow, C.L. Sun, V.C. Lo, and H.L.W. Chan, *Appl. Phys. Lett.* 92, 022901 (2008).
31. M.M. Vopson and S. Lepadatu, *Appl. Phys. Lett.* 105, 122901 (2014).